

Article

Hydroelastic Response of a Moored Floating Flexible Circular Structure Applying BIEM

Sarat Chandra Mohapatra *  and C. Guedes Soares 

Centre for Marine Technology and Ocean Engineering (CENTEC), Instituto Superior Técnico, Universidade de Lisboa, Av. Rovisco Pais, 1049-001 Lisboa, Portugal; c.guedes.soares@centec.tecnico.ulisboa.pt
* Correspondence: sarat.mohapatra@centec.tecnico.ulisboa.pt

Abstract: A hydroelastic model associated with the interaction between a surface wave and a floating circular structure connected with mooring lines in finite water depth is developed using BIEM. The BIEM solution is achieved using free surface Green's function and Green's theorem. Furthermore, the algebraic equations for circular structural displacement are derived from the integro-differential equation. The correctness of the BIEM code is verified with the results of shear force and deflection amplitude existing in the literature, and the hydroelastic response of the circular structure is analyzed. The comparison results show a good level of agreement between the present results and those from other calculations. It is observed that the shear force, bending moment, and deflection decrease for higher values of stiffness of the mooring lines. The current study may be supportive of the visualization of the effect of mooring stiffness and to generalize articulated circular structure models for ocean space utilization.

Keywords: circular flexible plate; BIEM; spring moorings; hydroelastic response; shear force; bending moment; deflection



Citation: Mohapatra, S.C.; Guedes Soares, C. Hydroelastic Response of a Moored Floating Flexible Circular Structure Applying BIEM. *J. Mar. Sci. Eng.* **2023**, *11*, 2322. <https://doi.org/10.3390/jmse11122322>

Academic Editors: Decheng Wan and Kamal Djidjeli

Received: 13 October 2023
Revised: 24 November 2023
Accepted: 6 December 2023
Published: 7 December 2023



Copyright: © 2023 by the authors. Licensee MDPI, Basel, Switzerland. This article is an open access article distributed under the terms and conditions of the Creative Commons Attribution (CC BY) license (<https://creativecommons.org/licenses/by/4.0/>).

1. Introduction

The interest in floating flexible offshore structures has been developing because of their applications in floating flexible platforms for wave energy production, floating offshore aquaculture bases, and floating breakwaters, among others. The study of the hydroelastic behavior of floating flexible structures has accepted a fair amount of recognition because of its cost-efficient, easy construction, and environmentally friendly qualities. Furthermore, due to the flexibility of such structures under wave excitations, their elastic deformations become more prominent than rigid-body motions. Hence, to perfectly estimate the displacement and wave quantity analysis of floating flexible structures, it is necessary to use hydroelastic analysis during the design phase [1].

Wave scattering via a floating horizontal flexible circular structure on a water-free surface is an interesting hydroelastic problem that has been investigated by many researchers based on the different approaches that the literature discusses in the subsequent paragraphs. In particular, in wave scattering, the understanding of the hydroelastic response of a floating flexible circular structure is relevant to many physical problems arising in ocean engineering, covering from offshore wave energy converters and solar wind devices to large floating structures and ice sheets [2]. Therefore, for the practical application of floating flexible circular structures in engineering design, the hydroelastic response to the effects of structural properties combined with mooring lines is essential for ensuring its safety and serviceability in the marine environment.

The connection of mooring lines of a floating flexible structure is essential for stabilizing the floating structure. Different types of mooring systems can be used for floating flexible structures. Nevertheless, this particular mooring system design depends on the environmental depths and conditions and the specific design of the floating flexible

structure [3–5]. When placing the very large floating structure (VLFS) in the intermediate depth, catenary-type, taut legs, elastic, and spring type of moorings are mostly used. In the context of the present work, spring mooring is connected to the circular floating flexible structure to stabilize a place or to avoid the drift of the floating structure.

Researchers use numerical methods to overcome the bulkiness of the computational load associated with a flexible structure with mooring systems. Often, investigators apply numerical methods and solutions to reduce these struggles. For instance, based on the BEM-FEM, the hydrodynamic force and elastic response of the floating body were calculated in [6]. Furthermore, the hydrodynamic coefficients from the BEM-FEM results were compared with the two-dimensional model results by conducting experiments. The wave-induced hydroelastic response in terms of the deflection of a VLFS was calculated based on the B-spline Galerkin scheme in [7]. The results of vertical deflections from the B-spline Galerkin scheme were compared with measurements and showed a good level of agreement. The deformation of the floating flexible structure was studied based on a nonlinear numerical method FEM and BEM for fluid motion [8]. The nonlinear numerical method was checked for three different types of waves against the experimental results. Based on the shallow water and thin plate theory, the wave responses via the shear force and bending moment of the rectangular plate were analyzed numerically [9]. The derivation of IDE and calculation of the deflection of VLFP using BEM were presented [10]. The reflection and transmission coefficients with zero current assumption were analyzed based on the BEM code simulations. Under different water depths, the hydroelastic response of VLFP via structural displacements, wave quantities, reflection, and transmission coefficients was analyzed using the BIEM code [11]. Using the boundary integral method, the water–wave interaction with a pontoon-type VLFS was investigated [12], and the results were compared with the MEFEM. Under different edge constraints, the hydroelastic waves of an ice-covered surface via wave celerity, wave profiles, and strain based on the elastic thin plate theory were investigated in [13].

Over the past few years, several studies on the various aspects of floating elastic circular plates have been reported in the literature under analytical and semi-analytical methods. For instance, under time domain analysis, the motion of a floating circular plate via structural deflections was investigated in [14] using the MEFEM. Under various water depths, the hydroelastic response of a floating circular plate was analyzed by an analytical and numerical methodology [15]. In this study, the solutions were obtained by involving Bessel's functions, IDE, Green's function, and free edge boundary conditions at the end of the structure. The response of an array of circular floating porous plates under the action of surface waves was analyzed based on a theoretical approach via the MEFEM [16]. They observed that energy dissipation could be enhanced by the hydrodynamic interaction between the elastic plates. The behavior of a floating elastic plate was analyzed numerically in a two-dimensional Cartesian coordinate system in finite water depth [17,18]. The numerical results had a good agreement with the experimental data and existing published numerical simulations.

Under the action of gravity waves and based on the thin elastic plate theory, the response of a single or pair of circular structures was reported in [19] by conducting a series of experiments. Under regular waves, the hydroelastic response on the deflections of the discs via natural modes and flexural motions of floating single and double discs was investigated based on modal analysis [20]. Under the action of external loads, the solution for incident waves on a circular elastic plate in three dimensions was provided in different water depths [21] to analyze the deflection of the circular plate. From this study, it was found that the inertial parameter influences the deflection amplitude of the circular plate slightly. The closed-form solutions on the interaction between waves and circular thin elastic plates were provided in the water of shallow [22] and finite depth [23]. From the contour plot, they observed that the plate and free surface deflections were different because of imposed transition conditions.

Under the action of a regular wave, the hydroelastic response of a circular VLFS was analyzed based on the Mindlin plate theory in [24,25] using the Rayleigh–Ritz method to solve the equation of motion. They presented the Benchmark solutions for deflections and stress-resultants of the circular VLFS.

Under the consideration of the axisymmetric unsteady formulation, the velocities of two circular plates were analytically studied in shallow water depth, and the results were validated against the experiments in [26]. A model associated with the interaction between sea waves and flexible circular ice floe was used to study the motion of the ice floe and validate the thin circular plate based on two different analytical methods [27]. They observed that the deformation of ice floes became easier for long-crested incoming waves than those of thicker ones. The mitigation of the hydroelastic response of floating circular VLFS was studied by attaching a submerged plate using analytical and numerical methods [28]. They confirmed that the motion of VLFS was reduced by the submerged plate effectively.

It is worth mentioning that the present BIEM simulation is conducted in a workstation with Intel® core i7-7700K CPU with a 4.20 GHz, 4201 Mhz, 4 Core(s), 8 Logical Processor(s), and 16 GB of RAM. Normally, for each case, the computation time is run for around 10–12 min. The current BIEM is one of the other approaches to study the hydroelastic response of this problem by consolidating structural displacements into the integro-differential equation that involves a less computational cost than in [29–31].

The previous work of the authors is relevant to the present paper in terms of the hydroelastic response of the floating flexible structure discussed below. The various aspects of the wave motion characteristics over a combined system of floating and submerged porous structures were discussed [32]. They found that the motion of waves is faster in the floating flexural mode than that of waves in the submerged flexural mode. Under Fourier transform with Green’s function technique, the formulae in series form as well as the integral form were presented in different water depths in 3D for a model of a floating and submerged flexible structure system [33]. On the other hand, recently, the hydroelastic response of a moored floating horizontal flexible plate was analyzed based on a BIEM model code [34]. They discussed the combined influence of the mooring stiffness and different design parameters related to the BIEM model under different water depths.

As studied in the above literature, to fill the gap, a hydroelastic model associated with the interaction between waves and a floating circular structure based on BIEM is formulated, and various effects on the hydroelastic response under design parameters are investigated.

Section 2 presents the model definition, including governing equations, structural equations, and boundary conditions, along with far-field conditions. Section 3 derives the integro-differential equation, including Bessel’s functions and structural edge conditions. In Section 4, the results of shear force and deflection amplitude are compared with the existing literature to verify the level of accuracy of the present code. Furthermore, the coupled effects of structural hydroelastic and mooring stiffness on the deflections, bending moment, and shear force are analyzed for different structural parameters, including flexural rigidity and compressive force with environmental depth, in detail. Section 5 provides the remarks from the present analysis, and future recommendations are summarized pointwise.

2. Definition of Problem Formulation

The hydroelastic model is formulated in a polar coordinate system where (r, θ, z) is the axis of the floater at $r = 0$ and $\theta = 0$ and is chosen to coincide with the incident wave propagation over finite depth $z = h$. A circular flexible structure (modelled based on the thin plate theory) of radius $r = a$ floating at $z = 0$ relates to spring mooring with stiffness q . Furthermore, the fluid characteristics are the same as in [34].

The entire water region is split into three regions described by the open water region and the circular structure covered region referred to as \mathcal{R}_O and \mathcal{R}_P , respectively (see Figure 1).

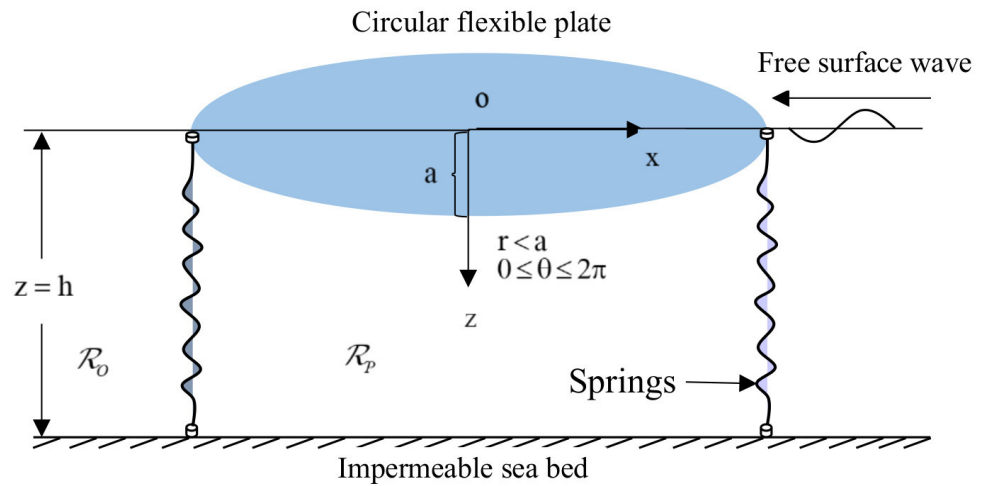


Figure 1. Hydroelastic model configuration.

Hence, the velocity potential is defined by $\Phi(r, \theta, z, t)$, satisfying the Laplacian in cylindrical coordinates as follows:

$$\left(\nabla_{r\theta}^2 + \frac{\partial^2}{\partial z^2} \right) \Phi(r, \theta, z; t) = 0, \tag{1}$$

where $\nabla_{r\theta}^2 = \left(\frac{\partial^2}{\partial r^2} + \frac{1}{r} \frac{\partial}{\partial r} + \frac{1}{r^2} \frac{\partial^2}{\partial \theta^2} \right)$ and

The linearized dynamic and free surface boundary conditions in \mathcal{R}_0 are given by the following:

$$\Phi_t + g\eta = 0 \text{ on } y = 0, r > a, \tag{2}$$

$$\frac{\partial^2 \Phi}{\partial t^2} - g \frac{\partial \Phi}{\partial z} = 0 \text{ on } y = 0, r > a, \tag{3}$$

where η and g denote the free surface elevation and the gravitational constant.

The condition at $z = h$ is given by

$$\frac{\partial \Phi}{\partial z} = 0, \tag{4}$$

The linearized condition in the region \mathcal{R}_p is obtained as

$$\left(\alpha \nabla_{r\theta}^4 + \beta \nabla_{r\theta}^2 + \rho_p d \frac{\partial^2}{\partial t^2} \right) \frac{\partial \Phi}{\partial z} = \rho \left(\frac{\partial^2 \Phi}{\partial t^2} - g \frac{\partial \Phi}{\partial z} \right) \text{ for } r < a, \tag{5}$$

where α represents the flexural rigidity of the circular flexible structure. β denotes the compressive force acting on the circular structure.

The following conditions yield from the moored edge condition at $r = a$ and $0 < \theta < 2\pi$ as follows:

The bending moment gives the following:

$$\alpha \left[\frac{\partial^2 \zeta}{\partial r^2} + \nu \left(\frac{1}{r} \frac{\partial \zeta}{\partial r} + \frac{1}{r^2} \frac{\partial^2 \zeta}{\partial \theta^2} \right) \right] = 0 \text{ for } r = a \text{ and } 0 < \theta < 2\pi. \tag{6}$$

The shear force yields

$$\left[\alpha \left\{ \frac{\partial}{\partial r} \nabla_{r\theta}^2 \zeta + \frac{(1-\nu)}{r^2} \left(\frac{\partial}{\partial r} - \frac{1}{r} \right) \frac{\partial^2 \zeta}{\partial \theta^2} \right\} + \beta \frac{\partial \zeta}{\partial r} \right] = q \text{ for } r = a \text{ and } 0 < \theta < 2\pi, \tag{7}$$

where $\zeta(r, \theta)$ is the circular structure deflection.

The far-field condition can be read as

$$\lim_{r \rightarrow \infty} \sqrt{r} \left(\frac{\partial \Phi_o}{\partial r} - ik_0 \Phi_o \right) = 0, \tag{8}$$

where Φ_o is the velocity potential in \mathcal{R}_o . The regions in \mathcal{R}_o and \mathcal{R}_p must be matched at $r = a$. Hence, the conditions along the interface of the circular boundary of \mathcal{R}_o and \mathcal{R}_p are given by the following:

$$\phi_O|_{r=a^-} = \phi_P|_{r=a^+}, \text{ continuity of pressure,} \tag{9}$$

$$\frac{\partial \phi_O}{\partial r} \Big|_{r=a^-} = \frac{\partial \phi_P}{\partial r} \Big|_{r=a^+}, \text{ continuity of velocity} \tag{10}$$

3. IDE Using the BIEM

The complex velocity potential $\phi_O(r, \theta, z)$ is expressed into the incident ϕ_I and the scattered potentials ϕ_S in \mathcal{R}_O as (see [34])

$$\phi_O(r, \theta, z) = \phi_I(r, \theta, z) + \phi_S(r, \theta, z), \tag{11}$$

where

$$\phi_I(r, \theta, z) = \frac{-igI_0}{2\omega} Y(z) e^{ik_0 r \cos \theta}, \tag{12}$$

with $Y(z) = \cosh k(h - z) / \cosh kh$, $r = \sqrt{x^2 + y^2}$, $\theta = \tan^{-1}(y/x)$ where $x = r \cos \theta$, $y = r \sin \theta$, and I_0 are the incident wave amplitude and k_0 satisfies $\ell = k \tanh kh$ with $\ell = \omega^2 / g$. It can be mentioned that the behavior of the roots of the dispersion relation can be found in [34].

Let the Green’s function $\mathcal{G}(r, \theta, z; u_0, v_0, w_0)$ with (u_0, v_0, w_0) and (r, θ, z) be the source point and any point in the water region. Hence, Green’s function $\mathcal{G}(r, \theta, z; u_0, v_0, w_0)$ at the free surface $z = w_0 = 0$ is obtained by applying Graf’s mathematical addition theorem to the Bessel function to the integrand as follows:

$$\mathcal{G}(r, \theta; u_0, v_0) = 2 \int_C \frac{k}{(\ell - k \tanh kh)} \sum_{q=0}^{\infty} \delta_q J_q(kr) J_q(ku_0) \cos q(v_0 - \theta) dk, \tag{13}$$

where

$$\delta_q = \begin{cases} 1 & \text{for } q = 0 \\ 2 & \text{for } q = 1, 2, 3, \dots \end{cases}$$

Proceeding similarly to [34], the integro-differential equation can be obtained as

$$\begin{aligned} & \left[\{ \alpha \nabla_{r\theta}^4 + \beta \nabla_{r\theta}^2 + (\rho g - m\omega^2) \} \frac{\partial \phi_P}{\partial z} \right] \\ & + \frac{\ell}{4\pi} \int_{\mathcal{R}_p} \left\{ (\alpha \nabla_{u_0 v_0}^4 + \beta \nabla_{u_0 v_0}^2 - m\omega^2) \left(\frac{\partial \phi_P}{\partial w_0} \right) \right\} \mathcal{G}(r, \theta; u_0, v_0) dr d\theta = \rho g \frac{\partial \phi_I}{\partial z}, \end{aligned} \tag{14}$$

where, ω is the angular frequency with a simple harmonic in time. Using Equations (2) and (3) and combining Equations (13) and (14), an IDE can be expressed in respect of $\zeta(r, \theta)$ as follows:

$$\begin{aligned} & \{ \alpha \nabla_{r\theta}^4 + \beta \nabla_{r\theta}^2 + (\rho g - m\omega^2) \} \zeta(r, \theta) \\ & + \frac{\ell}{4\pi} \int_{\mathcal{R}_p} (\alpha \nabla_{u_0 v_0}^4 + \beta \nabla_{u_0 v_0}^2 - m\omega^2) \zeta(u_0, v_0) \mathcal{G}(r, \theta; u_0, v_0) du_0 dv_0 = I_0 e^{ik_0 r \cos \theta}. \end{aligned} \tag{15}$$

where

$$\tilde{\zeta}(r, \theta) = \sum_{m=1}^M \sum_{n=0}^{\infty} A_{mn} J_n(\gamma_m r) \cos n\theta, 0 < x < b, 0 < \theta < 90^\circ, \tag{16}$$

where $J_n(\gamma_m r)$ represents the Bessel functions, A_{mn} s are the unknown amplitudes, and γ_m s are the wave numbers satisfying the dispersion relation (see [34])

$$\{\alpha\gamma_m^4 + \beta\gamma_m^2 + (\rho g - m\omega^2)\} \gamma_m \tanh \gamma_m h - \ell = 0. \tag{17}$$

The behavior of the roots associated with the relation (17) is similar to that discussed in [34], and 10 different roots are used to develop the present numerical BIEM code. Furthermore, the root characteristics are shown in Figure 2.

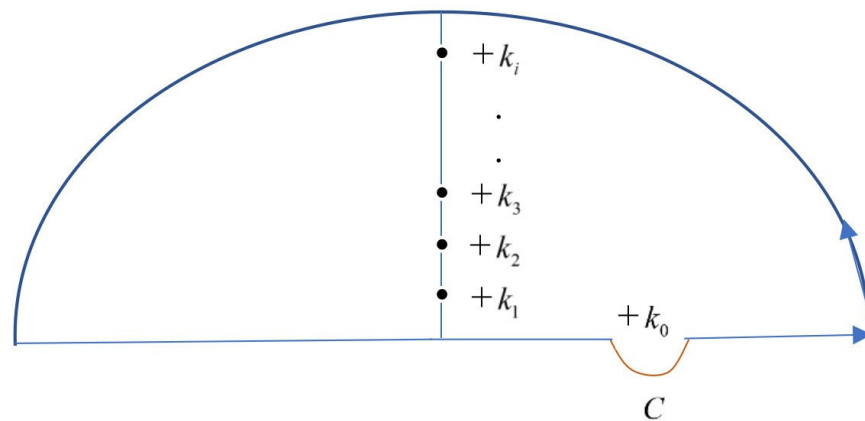


Figure 2. Closer integration contour.

Now, the IDE in terms of structural deflection at the free surface $z = 0$ is obtained by substituting the plate deflection form (16) and $\mathcal{G}(r, \theta, z; u_0, v_0, w_0)$ as defined in Equation (13) into expression (15) as follows:

$$\begin{aligned} & \{\alpha \nabla_{r\theta}^4 + \beta \nabla_{r\theta}^2 + (\rho g - m\omega^2)\} \sum_{m=1}^M \sum_{n=0}^{\infty} A_{mn} J_n(\gamma_m r) \cos n\theta \\ & + \frac{\ell}{4\pi} \int_0^a \int_0^a (\alpha \nabla_{u_0 v_0}^4 + \beta \nabla_{u_0 v_0}^2 - m\omega^2) \sum_{m=1}^M \sum_{n=0}^{\infty} A_{mn} J_n(\gamma_m u_0) \cos n v_0 \\ & \times 2 \int_C \frac{k}{(\ell - k \tanh kh)} \sum_{q=0}^{\infty} \delta_q J_q(k u_0) J_q(k r) \cos q(v_0 - \theta) u_0 du_0 dv_0 \\ & = I_0 \sum_{n=0}^N \varepsilon_n J_n(k_0 r) \cos n\theta. \end{aligned} \tag{18}$$

For the integration with respect to u_0 and v_0 with Equation (18), a set of $N + 1$ set of equations is provided as follows:

$$\begin{aligned} & \sum_{m=1}^M \{\alpha \gamma_m^4 + \beta \gamma_m^2 + (\rho g - m\omega^2)\} A_{mn} J_n(\gamma_m r) - \ell a \int_{\mathcal{R}_p} \sum_{m=1}^M (\alpha \gamma_m^4 + \beta \gamma_m^2 - m\omega^2) A_{mn} J_n(kr) \\ & \times 2 \int_C f(k) \frac{1}{(k^2 - \gamma_m^2)} [k J_{n+1}(ka) J_n(\gamma_m a) - \gamma_m J_n(ka) J_{n+1}(\gamma_m a)] dk = I_0 \varepsilon_n J_n(k_0 a). \end{aligned} \tag{19}$$

where $f(k) = k / (\ell - k \tanh kh)$.

Based on the complex function theory using the residue theorem to overcome the singularity under the integrals as in Equation (19), the poles of $f(k)$ are the roots of the relation (below Equation (12)) in \mathcal{R}_O . There are two real roots $k = \pm k_0$ and many imaginary roots are of the form $\pm ik$. Here, keeping in mind the physical nature of the problem and to

close the contour of the integration, the positive real root $k = +k_0$ and positive imaginary roots $k = +ik_i$ are taken into account to solve the problem, as shown in Figure 2. Therefore, following the procedure of [34], Equation (19) is rederived as follows:

$$\sum_{m=1}^M \{ \alpha \gamma_m^4 + \beta \gamma_m^2 + (\rho g - m\omega^2) \} A_{mn} J_n(\gamma_m r) - \ell a \int_{-\infty}^{+\infty} \sum_{m=1}^M (\alpha \gamma_m^4 + \beta \gamma_m^2 - m\omega^2) A_{mn} \frac{J_n(kr)}{(k^2 - \gamma_m^2)} \times \sum_{i=0}^{M-3} \frac{k_i^2}{(\alpha_i^2 h - \ell^2 h + \ell)(k - k_i)} [k J_{n+1}(ka) J_n(\gamma_m a) - \gamma_m J_n(ka) J_{n+1}(\gamma_m a)] dk = I_0 \epsilon_n J_n(k_0 a). \tag{20}$$

Under the application of the Cauchy theorem to the integral closed in the upper half-plane, in the case of the circular plate region $r < a$, the amplitudes A_{mn} are obtained by solving the system of $N + 1$ equations as follows:

$$\pi i \ell a \sum_{m=1}^M \frac{A_{mn} \alpha_0^2}{(k_0^2 h - \ell^2 h + \ell)(k_0^2 - \gamma_m^2)} \{ \alpha \gamma_m^4 + \beta \gamma_m^2 + (\rho g - m\omega^2) \} \times [k_0 H_{n+1}^{(1)}(k_0 a) J_n(\gamma_m a) - \gamma_m H_n^{(1)}(k_0 a) J_{n+1}(\gamma_m a)] = I_0 \epsilon_n. \tag{21}$$

Furthermore, a set of $(M - 3)(N + 1)$ equations are obtained by involving the poles at the imaginary axis as follows:

$$\pi i \ell a \sum_{m=1}^M \frac{A_{mn} k_i^2}{(k_i^2 h - \ell^2 h + \ell)(k_i^2 - \gamma_m^2)} \{ \alpha \gamma_m^4 + \beta \gamma_m^2 + (\rho g - m\omega^2) \} \times [k_i H_{n+1}^{(1)}(k_i a) J_n(\gamma_m a) - \gamma_m H_n^{(1)}(k_i a) J_{n+1}(\gamma_m a)] = 0. \tag{22}$$

Furthermore, conditions (6) and (7) give

$$\sum_{m=1}^M EI \left[\{ \gamma_m^2 - (n^2/a^2)v \} J_n(\gamma_m a) + (v/a) \gamma_m J_{n+1}(\gamma_m a) \right] = 0, \tag{23}$$

$$\sum_{m=1}^M EI \{ J_{n+1}(\gamma_m a) [\gamma_m^3 + n^2 \{ (v - 1)/a^2 \} \gamma_m] + [(\gamma_m^2/a) - \{ (1 + n^2)/a^2 \} \gamma_m + \{ (2n^2 + n^2(1 - v))/a^3 \} J_n(\gamma_m a)] \} A_{mn} + \sum_{m=1}^M f_c \gamma_m J_n(\gamma_m a) A_{mn} - q = 0 \tag{24}$$

where $i = 1, \dots, M - 1$.

The bending moment and shear force can be computed from the following formula:

$$M_B = \alpha \left[\frac{\partial^2}{\partial r^2} + \frac{v}{r} \left(\frac{\partial}{\partial r} + \frac{1}{r} \frac{\partial^2}{\partial \theta^2} \right) \right] \zeta(r, \theta). \tag{25}$$

$$F_S = \left[\alpha \left\{ \frac{\partial}{\partial r} \nabla_{r\theta}^2 + \frac{(1 - v)}{r^2} \left(\frac{\partial}{\partial r} - \frac{1}{r} \right) \frac{\partial^2}{\partial \theta^2} \right\} + \beta \frac{\partial}{\partial r} \right] \zeta(r, \theta) - q \tag{26}$$

where $\zeta(r, \theta)$ is the same as in Equation (16).

4. Comparison Results and Analysis

The results of the shear force, bending moment, and deflections are presented for the hydroelastic response of the circular structure on different design parameters; these include the mooring stiffness, flexural rigidity, compressive force, water depth, and the angle of incidence for the engineering practice cases.

The BIEM codes are developed by incorporating Bessel functions and considering 15 terms in the series solution to compute the deflections, shear force, and bending moments of the circular flexible structure. Hereafter, the design parametric values of the gravitational constant and water density are $g = 9.8 \text{ ms}^{-2}$ and $= 1025 \text{ kg/m}^3$ unless mentioned otherwise.

In Figure 3, the result of the present shear force with the MEM [24] against λ/a is compared for $\alpha = 10^6$, $\beta = 1.2\sqrt{EI\rho g}$, $h/a = 0.5$, $q = 10^{0.05} \text{ Nm}^{-1}$ (low value), and the +ve half of the non-dimensional wavelength λ/a is selected. The results from Figure 3 indicate that the present BIEM code agrees well with the other calculation model [24]. Nevertheless, a very small discrepancy occurs due to the formulation under the assumption of the thin plate theory and the Mindlin plate theory in [24]. Hence, it is suspected that model [24] produces a smaller shear force for a longer wavelength that the present code cannot emulate.

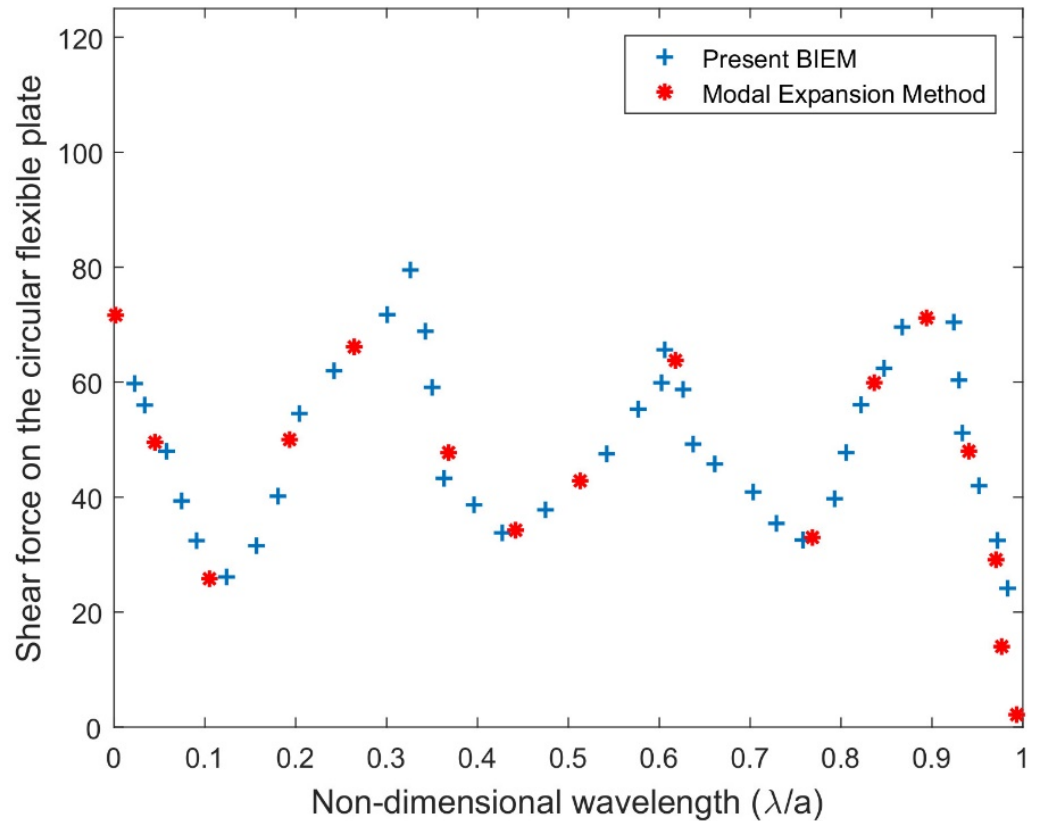


Figure 3. Comparison of shear force between BIEM and the result [24].

Additionally, in Figure 3, the shear force from the Modal Expansion Method [24] is 66.19 m, while the current BIEM code is 80.08 m, which is 11.58% lower.

In Figure 4, the result of the present deflection amplitude with the model without plate condition [28] against r/λ is compared for $\alpha = 10^5$, $\beta = 2\sqrt{EI\rho g}$, $h/a = 0.8$, and $q = 10^{4.5} \text{ Nm}^{-1}$ is selected. From Figure 4, it is observed that the deflection amplitude from the present BIEM code agrees well with the other calculation model [28].

Figure 5 compares the deflection of freely and moored floating circular structures versus the non-dimensional wavenumber ka . The values of the deflection of a moored circular structure become much lower than that of the freely floating one, which means a moored floating circular plate is more stable than a free one. In addition, in Figure 5, the deflection amplitude in the case of the freely floating structure is 0.097 m, while the moored one is 0.043 m, which is 54% larger.

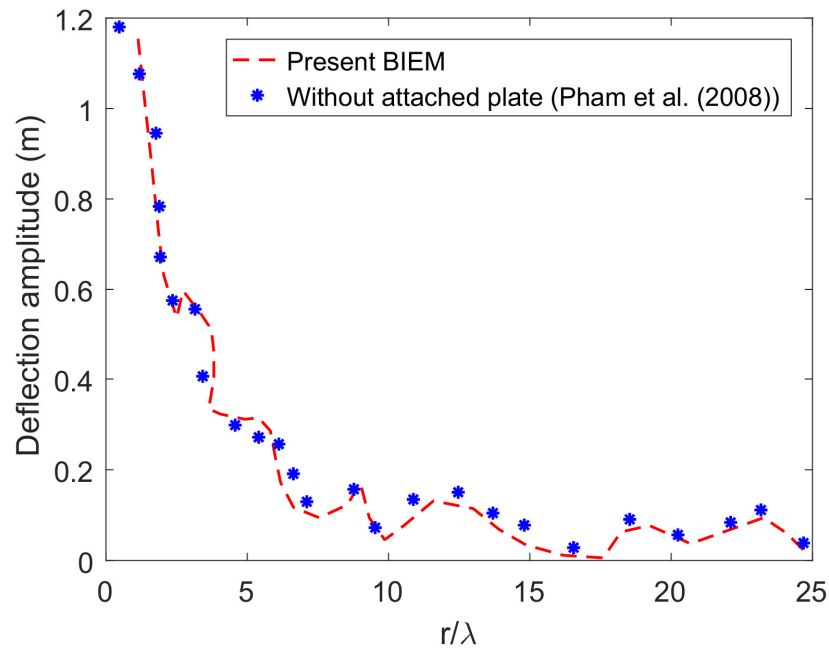


Figure 4. Comparison of deflection amplitude between BIEM and the result [28].

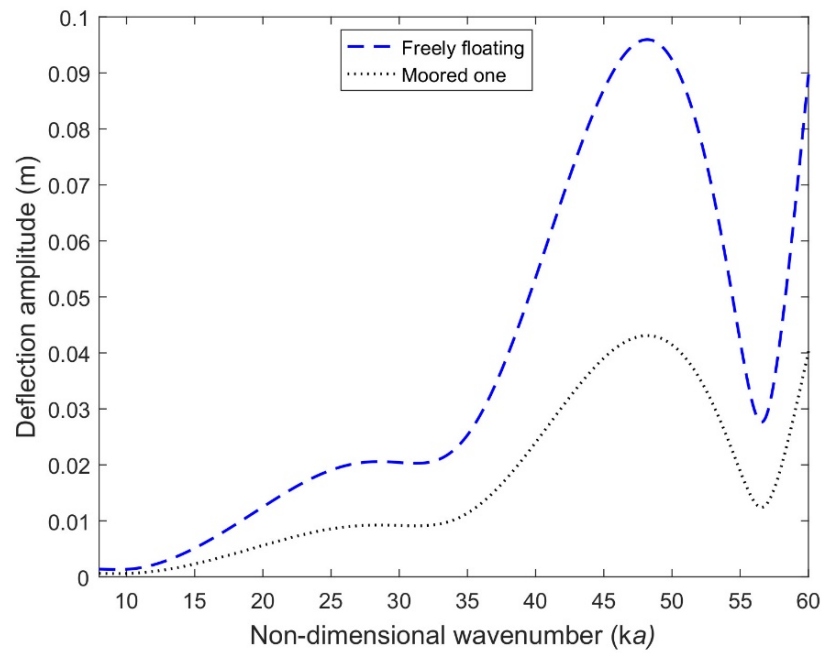
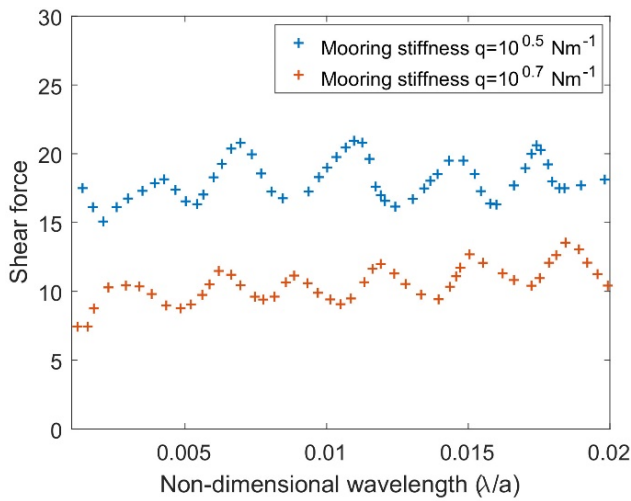
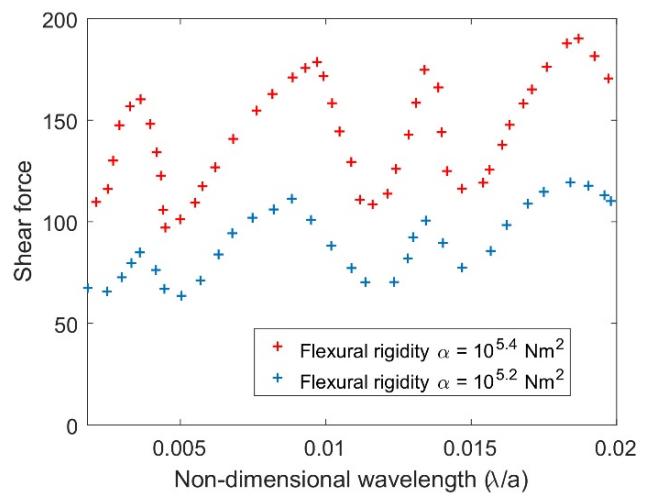


Figure 5. Comparison between freely floating and moored structures (spring stiffness $q = 10^5 \text{ Nm}^{-1}$) with $h/a = 0.5$.

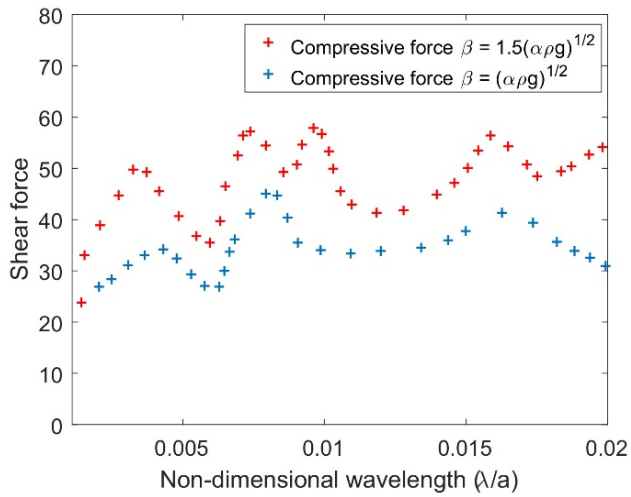
Figure 6 simulates the effects of shear force on the circular structure for various (a) mooring stiffness, (b) flexural rigidity, (c) compressive force, and (d) water depth values against the non-dimensional wavelength with mooring stiffness $q = 0.5 \text{ Nm}^{-1}$. In Figure 6a,d, the values of shear force decrease for larger mooring stiffness and deep water depth. This can be explained as more wave energy passing below the structure leads to less shear force acting on the circular structure. In addition, in Figure 6a, the shear force from the mooring stiffness value $q = 10^{0.5} \text{ Nm}^{-1}$ is 20.779 m, whilst the mooring stiffness value $q = 10^{0.7} \text{ Nm}^{-1}$ is 11.337, which is 31.47% larger.



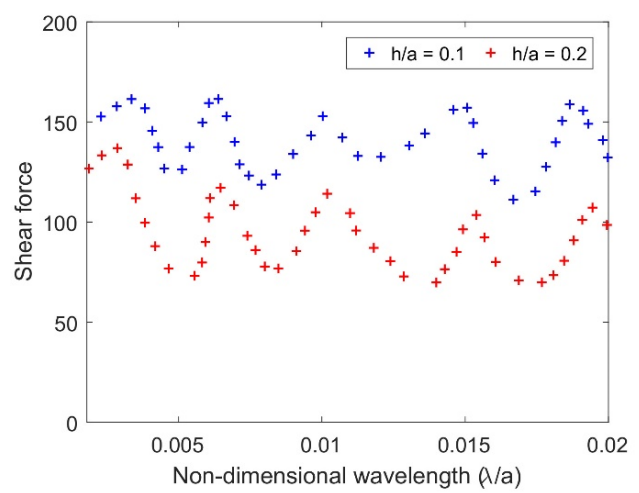
(a) Influence of mooring stiffness q



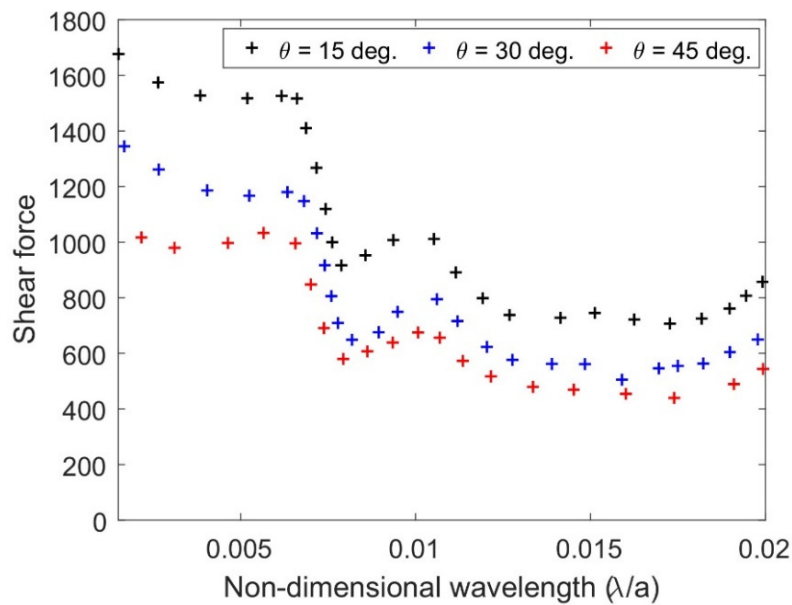
(b) Influence of flexural rigidity α



(c) Influence of compressive force β



(d) Influence of water depth h/a



(e) Influence of incidence angle θ

Figure 6. Variation in shear force on different q , α , β , and h/a versus λ/a with $\alpha = 10^5$, $\beta = 1.5\sqrt{EI\rho g}$.

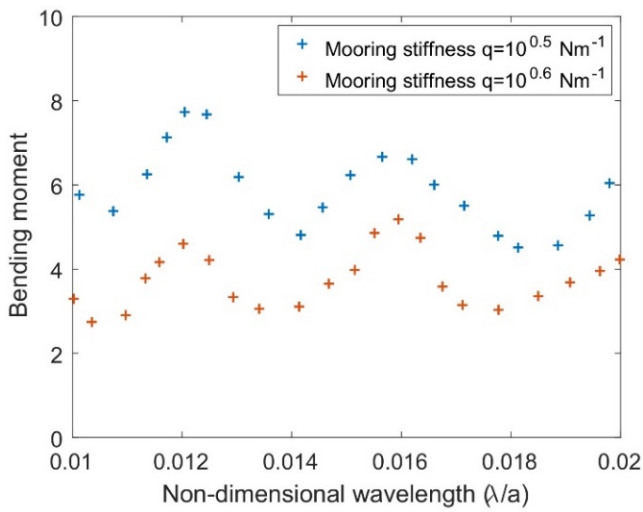
From Figure 6b,c, the shear force decreases for decreasing values of flexural rigidity and compressive force. The reasons are similar to those in [34]. In Figure 6e, with increasing θ , the shear force becomes lower. Nevertheless, as the non-dimensional wavelength increases, the resonating pattern decreases in nature (as in [34]). Furthermore, in Figure 6e, the shear force from $\theta = 15$ deg. is 1686.167 m, whilst from $\theta = 30$ deg., it is 1348.146 m, which is 18.77% greater. Also, at $\theta = 45$ deg., the shear force is 1013.594 m, which is 18.58% smaller than that of $\theta = 30$ deg. and 37.36% smaller than that of $\theta = 15$ deg.

Figure 7 shows the effects of (a) q , (b) α , (c) β , (d) h/a , and (e) θ on the bending moments vs. λ/a . It is clear that, for larger values of q and α , the bending moment amplitude of the circular structure becomes lower. This is because α and q decrease the flexibility of the circular structure that contributes to the hardness, which accelerates to low bending. Moreover, in Figure 6b, it can be explained that the bending behavior of the flexible structure depends on the structural rigidity and the continuous excitation of the waves at the upstream region. The bending behavior depends on the flexibility of the structure and the continuous excitation of waves in the upstream region. Furthermore, in Figure 7a, the bending moment from the mooring stiffness value $q = 10^{0.5} \text{ Nm}^{-1}$ is 7.797 m, whilst from the mooring stiffness value $q = 10^{0.6} \text{ Nm}^{-1}$ is 4.646, which is 31.51% larger. On the other hand, for the larger values of β and h/a , the bending moment decreases for reasons similar to Figure 6b,d. In Figure 7e, in general, it may be mentioned that the pattern of results for the bending moment on different θ are similar to that of Figure 6e. However, the values of bending moments for different θ are lower than that of the shear forces seen in Figure 6e.

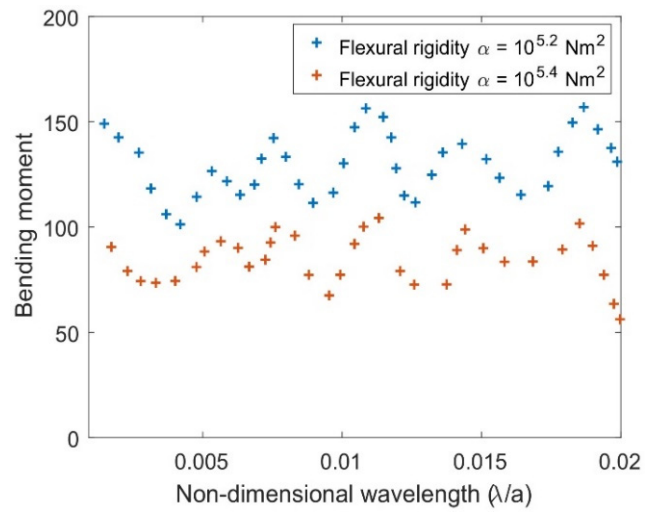
Additionally, in Figure 7e, the bending moment from $\theta = 15$ deg. is 119.565 m, whilst, from $\theta = 30$ deg., it is 102.025, which is 14.032% larger. Also, $\theta = 45$ deg., and the bending moment is 55.830 m, which is 36.97% smaller than that of $\theta = 50$ deg. and 50.98% smaller than that of $\theta = 15$ deg.

In Figure 8, the influences of various parameters (a) q , (b) α , (c) β , (d) h/a , and (e) θ on the deflection amplitude of the circular structure against the dimensionless wavenumber (ka) are plotted with $\alpha = 10^5$, $\beta = 1.5\sqrt{EI\rho g}$. In Figure 8a, with the increase in mooring stiffness q , the circular structure deflection decreases which is because as the mooring stiffness increases, the flexible structure becomes harder, which accelerates to low deflection. In Figure 8b, the deflection of the circular flexible structure decreases with an increase in α . The reasons are similar to Figure 8a. Moreover, in Figure 8a, the deflection amplitude from the mooring stiffness value $q = 10^{4.5} \text{ Nm}^{-1}$ is 0.0947 m, whilst from the mooring stiffness value $q = 10^{5.5} \text{ Nm}^{-1}$ is 0.0751, which is 19.6% larger. On the other hand, the deflection amplitude from the mooring stiffness value $q = 10^{6.5} \text{ Nm}^{-1}$ is 0.0429 m, which is 32.2% smaller than that of $q = 10^{5.5} \text{ Nm}^{-1}$ and 51.8% smaller than that of $q = 10^{4.5} \text{ Nm}^{-1}$.

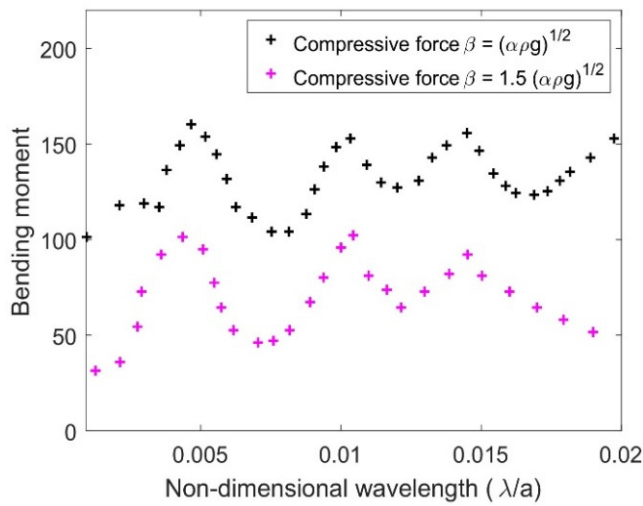
In Figure 8c, the structural deflection becomes higher for larger values of β acting on the floating circular structure. This shows that, with a particular value of q , the compressive force changes the shape of the floating flexible circular structure. In Figure 8d, the deflection amplitude decreases with an increase in h/a . The variations are negligible for different non-dimensional water depths for lower values of the wavenumber, whilst this effect is as significant as the values of the wavenumber are higher. In Figure 8e, the deflection amplitude decreases with an increase in θ which is because when the incident wave becomes perpendicular to the floating circular structure, it propagates along the floating horizontal circular structure in the radial direction. Furthermore, it can be explained that as the angle of incidence increases, there is an effect on the incoming wave of the circular floating flexible structure. This observation is similar to [34] in the case of floating and submerged flexible plate configurations.



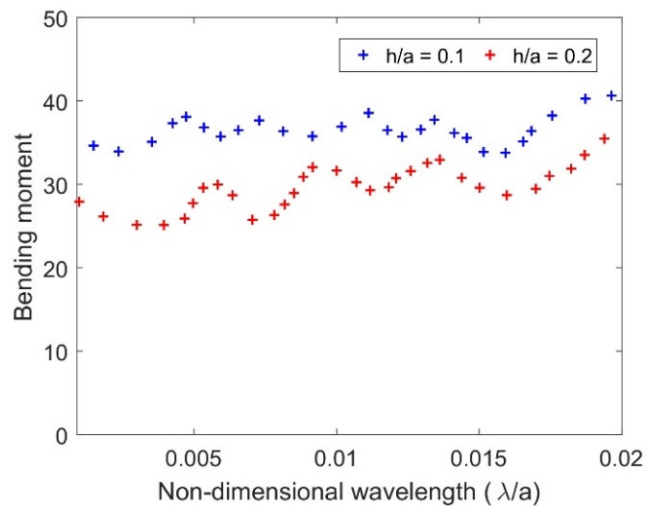
(a) Influence of mooring stiffness q



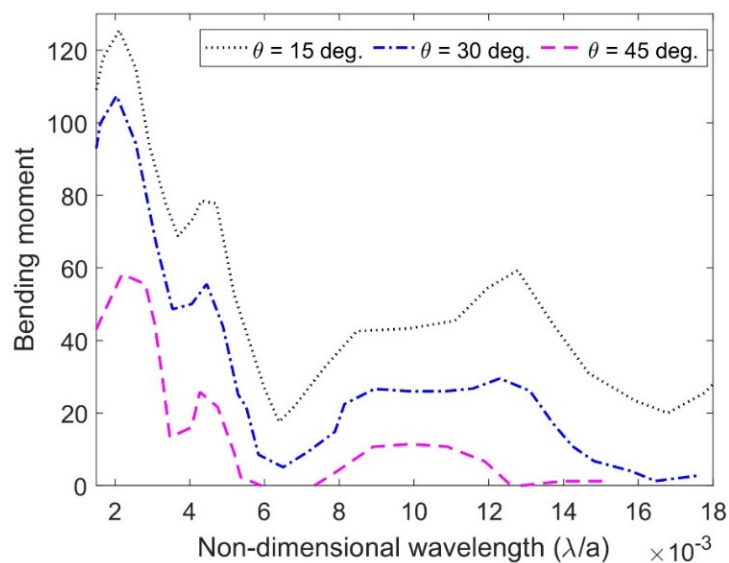
(b) Influence of flexural rigidity α



(c) Influence of compressive force β

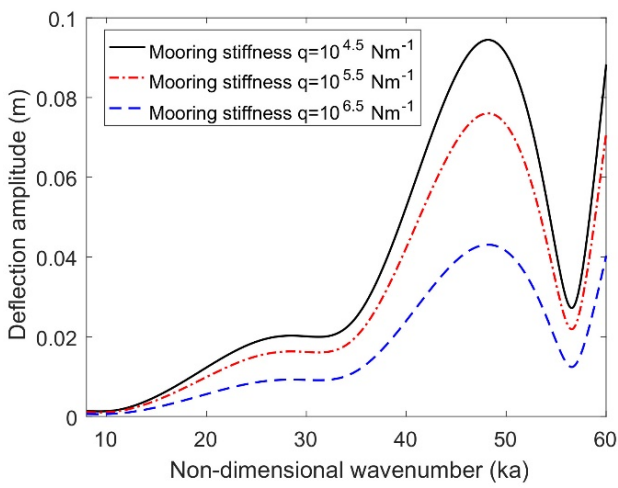


(d) Influence of water depth h/a

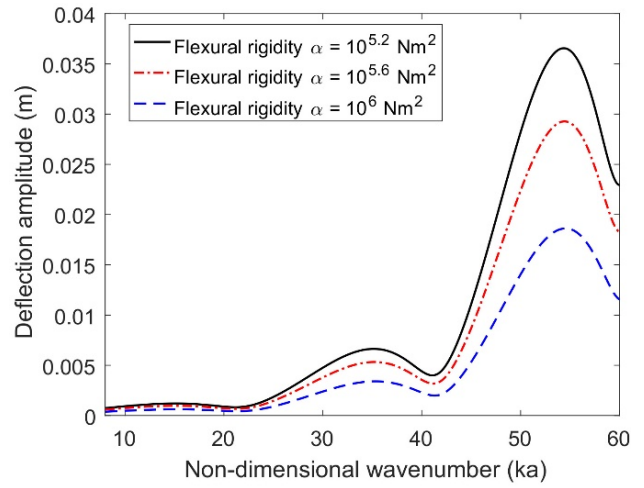


(e) Influence of incidence angle θ

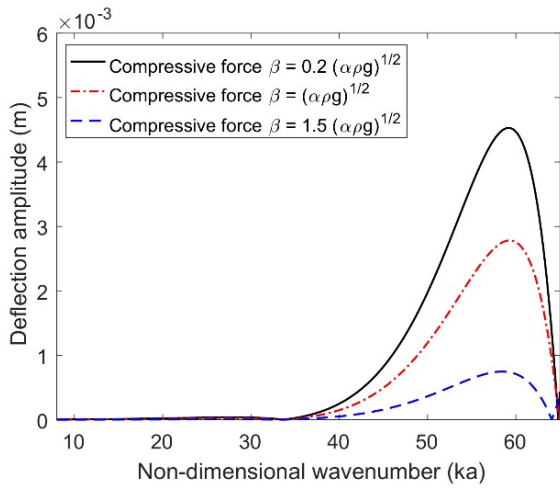
Figure 7. Variations in shear force on different q , α , β , h/a , and θ versus λ/a with $\alpha = 10^5$, $\beta = 1.5\sqrt{EI\rho g}$.



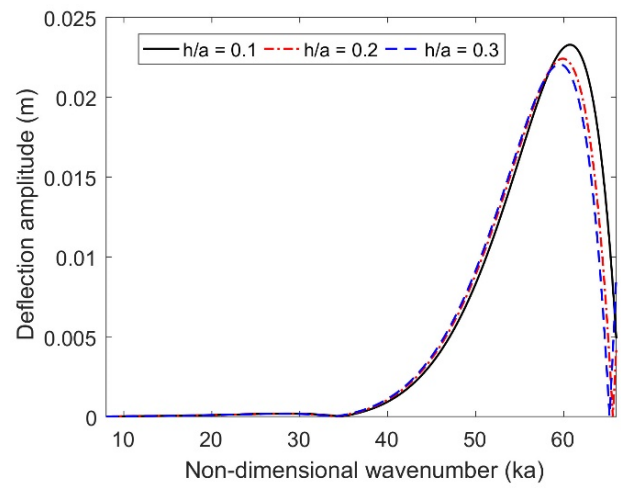
(a) Influence of mooring stiffness q



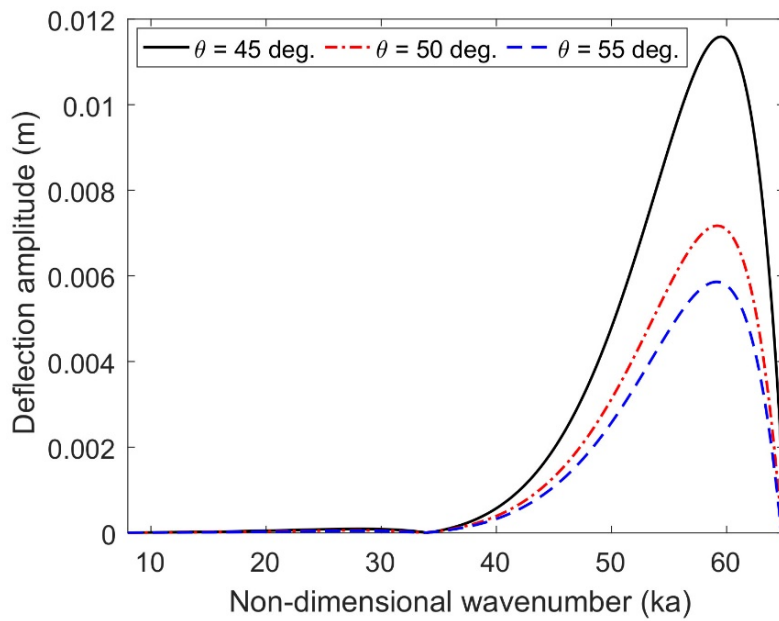
(b) Influence of flexural rigidity α



(c) Influence of compressive force β



(d) Influence of water depth h/a



(e) Effect of θ on deflection amplitude

Figure 8. Variations in deflection amplitude on different q , α , β , and h/a versus λ/a .

Furthermore, in Figure 8e, the deflection amplitude from the angle of incidence $\theta = 45$ deg. is 0.0116 m, whilst from $\theta = 50$ deg., it is 0.0072, which is 36.66% larger. On the other hand, the deflection amplitude from $\theta = 55$ deg. is 0.0058 m, which is 11.66% smaller than that of $\theta = 50$ deg. and 48.33% smaller than that of $\theta = 45$ deg.

5. Conclusions

A novel BIEM model for wave interaction with a circular floating flexible structure connected with mooring lines is established. The system of linear equations associated with IDE is presented along with the moored conditions. To ensure the accuracy of the computation, the present BIEM model code is validated with one MEM model result. Further, the hydroelastic response of the moored circular structure is analyzed via the shear force, bending moment, and deflections for different design parameters. The main conclusions are summarized as follows:

1. The BIEM model formulation for a flexible circular structure connected with mooring lines under the compressive force and its hydroelastic response is one of the advanced studies in the literature.
2. It was found that the BIEM code result is supported by the MEM model formulations.
3. With an increase in the stiffness of the mooring lines, the shear force and bending moment become lower. A similar effect is observed in the case of the flexural rigidity of the circular plate.
4. In the case of the angle of incidence, for larger values of the incidence angle θ , the values of shear force and bending moment are lowered. Nevertheless, the bending moment has a lower value than that of shear force with respect to the angle of incidence.
5. It was also observed that the deflection amplitude decreases with an increase in the stiffness of the mooring lines, compressive force, water depth, angle of incidence, and the flexural rigidity of the floating circular structure.
6. The analysis of the hydroelastic response recommended that, for higher values of mooring stiffness, the deflection pattern of the circular structure decreases in nature. This deduced that the appropriate values of stiffness of the mooring lines q , compressive force β , angle of incidence θ , and flexural rigidity α play an important role in modeling a safe and reliable floating platform.

As a future scope, the present BIEM formulation and analysis might be useful to gain the knowledge to model VLFSs for ocean space utilization.

Author Contributions: Conceptualization, S.C.M. and C.G.S.; Methodology, S.C.M.; writing—original manuscript, S.C.M. and C.G.S. All authors have read and agreed to the published version of the manuscript.

Funding: This work contributes to the project HYDROELASTWEB—Hydroelastic behavior of horizontal flexible floating structures for applications to Floating Breakwaters and Wave Energy Converters, which is funded by the Portuguese Foundation for Science and Technology (Fundação para a Ciência e a Tecnologia—FCT) under contract 031488_770 (PTDC/ECI-EGC/31488/2017). The first author has been contracted as a Researcher by the Portuguese Foundation for Science and Technology (Fundação para a Ciência e Tecnologia—FCT), through Scientific Employment Stimulus, Individual support under the contract No. CEECIND/04879/2017. This work also contributes to the Strategic Research Plan of the Centre for Marine Technology and Ocean Engineering (CENTEC), which is financed by the Portuguese Foundation for Science and Technology (Fundação para a Ciência e Tecnologia—FCT) under contract UIDB/UIDP/00134/2020.

Institutional Review Board Statement: Not applicable.

Informed Consent Statement: Not applicable.

Data Availability Statement: Data are contained within the article.

Conflicts of Interest: The authors declare no conflict of interest.

Abbreviations

| | |
|-------|--|
| BIEM | Boundary Integral Equation Method |
| IDE | Integro-Differential Equation |
| FEM | Finite Element Method |
| BEM | Boundary Element Method |
| VLFS | Very Large Floating Structure |
| VLFP | Very Large Floating Platform |
| MEM | Modal Expansion Method |
| CPU | Central Processing Unit |
| MEFEM | Matched Eigenfunction Expansion Method |

References

1. Watanabe, E.; Utsunomiya, T.; Wang, C.M.; Xiang, Y. Hydroelastic analysis of pontoon-type circular VLFS. In Proceedings of the 13th International Offshore and Polar Engineering Conference, Honolulu, HI, USA, 25–30 May 2003; Volume 1, pp. 93–99.
2. Michele, S.; Zheng, S.; Buriyani, F.; Borthwick, A.G.L.; Greaves, D.M. Floating hydroelastic circular plate in regular and irregular waves. *Eur. J. Mech. B/Fluids* **2023**, *99*, 148–162. [[CrossRef](#)]
3. Jin, C.; Kim, G.J.; Kim, S.J.; Kim, M.; Kwak, H.G. Discrete-module-beam-based hydroelasticity simulations for moored submerged floating tunnel under regular and random wave excitations. *Eng. Struct.* **2023**, *275*, 115198. [[CrossRef](#)]
4. Bispo, I.B.S.; Mohapatra, S.C.; Guedes Soares, C. Numerical analysis of a moored very large floating structure composed by a set of hinged plates. *Ocean Eng.* **2022**, *253*, 110785. [[CrossRef](#)]
5. Amouzadrad, P.; Mohapatra, S.C.; Guedes Soares, C. Hydroelastic Response to the Effect of Current Loads on Floating Flexible Offshore Platform. *J. Mar. Sci. Eng.* **2023**, *11*, 437. [[CrossRef](#)]
6. Utsunomiya, T.; Watanabe, E.; Wu, C.; Hayashi, N.; Nakai, K.; Sekita, K. Wave response analysis of a flexible floating structure by BEM-FEM combination method. In Proceedings of the 5th International Offshore and Polar Engineering Conference, The Hague, The Netherlands, 11–16 June 1995; Volume 3, p. 400405.
7. Kashiwagi, M. A B-spline Galerkin scheme for calculating hydroelastic response of a very large floating structure in waves. *J. Mar. Sci. Technol.* **1998**, *3*, 37–49. [[CrossRef](#)]
8. Liu, X.; Sakai, S. Nonlinear analysis on the interaction of waves and flexible floating structure. In Proceedings of the 10th International Offshore and Polar Engineering Conference, Seattle, WA, USA, 28 May–2 June 2000.
9. Tsubogo, T. Wave response of rectangular plates having uniform flexural rigidities floating on shallow water. *Appl. Ocean Res.* **2006**, *28*, 161–170. [[CrossRef](#)]
10. Hermans, A.J. A boundary element method for the interaction of free-surface waves with a very large floating flexible platform. *J. Fluids Struct.* **2000**, *14*, 943–956. [[CrossRef](#)]
11. Andrianov, A.I.; Hermans, A. The influence of water depth on the hydroelastic response of a very large floating platform. *Mar. Struct.* **2003**, *16*, 355–371. [[CrossRef](#)]
12. Hegarty, G.M.; Squire, V.A. A boundary integral equation method for the interaction of large amplitude ocean waves with a compliant floating raft such as sea-ice floe. *J. Eng. Math.* **2008**, *62*, 355–372. [[CrossRef](#)]
13. Ren, K.; Wu, G.X.; Li, Z.F. Hydroelastic waves propagating in an ice-covered channel. *J. Fluid Mech.* **2020**, *886*, A18. [[CrossRef](#)]
14. Meylan, M.H. Time-Dependent Motion of a Floating Circular Elastic Plate. *Fluids* **2021**, *6*, 29. [[CrossRef](#)]
15. Andrianov, A.I.; Hermans, A.J. Hydroelasticity of a circular plate on water of finite or infinite depth. *J. Fluids Struct.* **2005**, *20*, 719–733. [[CrossRef](#)]
16. Zheng, S.; Meylan, M.; Zhu, G.; Greaves, D.; Iglesias, G. Hydroelastic interaction between water waves and an array of circular floating porous elastic plates. *J. Fluid Mech.* **2020**, *900*, A20. [[CrossRef](#)]
17. Korobkin, A. Numerical and asymptotic study of the two-dimensional problem on hydroelastic behavior of a floating plate in waves. *J. Appl. Mech. Tech. Phys.* **2000**, *41*, 286–293. [[CrossRef](#)]
18. Khabakhpasheva, T.I.; Korobkin, A.A. Hydroelastic behaviour of compound floating plate in waves. *J. Eng. Math.* **2002**, *44*, 21–40. [[CrossRef](#)]
19. Montiel, F.; Bonnefoy, F.; Ferrant, P.; Bennetts, L.G.; Squire, V.A.; Marsaul, P. Hydroelastic response of floating elastic discs to regular waves. part 1. wave basin experiments. *J. Fluid Mech.* **2013**, *723*, 604–628. [[CrossRef](#)]
20. Montiel, F.; Bennetts, L.G.; Squire, V.A.; Bonnefoy, F.; Ferrant, P. Hydroelastic response of floating elastic discs to regular waves. part 2. modal analysis. *J. Fluid Mech.* **2013**, *723*, 629–652. [[CrossRef](#)]
21. Sturova, I.V. The action of an unsteady external load on a circular elastic plate floating on shallow water. *J. Appl. Math. Mech.* **2003**, *67*, 407–416. [[CrossRef](#)]
22. Zilman, G.; Miloh, T. Hydroelastic buoyant circular plate in shallow water: A closed form solution. *Appl. Ocean Res.* **2000**, *22*, 191–198. [[CrossRef](#)]
23. Peter, M.A.; Meylan, M.H.; Chung, H. Wave scattering by a circular elastic plate in water of finite depth: A closed form solution. *Int. J. Offshore Polar Eng.* **2004**, *14*, 81–85.

24. Watanabe, E.; Utsunomiya, T.; Wang, C.M.; Hang, L.T.T. Benchmark hydroelastic responses of a circular VLFS under wave action. *Eng. Struct.* **2006**, *28*, 423–430. [[CrossRef](#)]
25. Wang, C.; Xiang, Y.; Watanabe, E.; Utsunomiya, T. Mode shapes and stress-resultants of circular Mindlin plates with free edges. *J. Sound Vib.* **2004**, *276*, 511–525. [[CrossRef](#)]
26. Korobkin, A.A.; Ohkusu, M. Impact of two circular plates one of which is floating on a thin layer of liquid. *J. Eng. Math.* **2004**, *50*, 343–358. [[CrossRef](#)]
27. Meylan, M.; Squire, V. Response of a circular ice floe to ocean waves. *J. Geophys. Res.* **1996**, *101*, 8869–8884. [[CrossRef](#)]
28. Pham, D.C.; Wang, C.M.; Utsunomiya, T. Hydroelastic analysis of pontoon-type circular VLFS with an attached submerged plate. *Appl. Ocean Res.* **2008**, *30*, 287–296. [[CrossRef](#)]
29. Simpson, R.N.; Bordas, S.P.A.; Trevelyan, J.; Rabczuk, T. A two-dimensional isogeometric boundary element method for elastostatic analysis. *Comput. Methods Appl. Mech. Eng.* **2012**, *209*, 87–100. [[CrossRef](#)]
30. Guo, H.; Zhuang, X.; Rabczuk, T. A deep collocation method for the bending analysis of Kirchhoff plate. *Comput. Mater. Contin.* **2019**, *59*, 433–456. [[CrossRef](#)]
31. Samaniego, E.; Anitescu, C.; Goswami, S.; Nguyen-Thanh, V.M.; Guo, H.; Hamdia, K.; Zhuang, X.; Rabczuk, T. An energy approach to the solution of partial differential equations in computational mechanics via machine learning: Concepts, implementation and applications. *Comput. Methods Appl. Mech. Eng.* **2020**, *362*, 112790. [[CrossRef](#)]
32. Mohapatra, S.C.; Guedes Soares, C. Hydroelastic Response to Oblique Wave Incidence on the Floating Plate with a Submerged Perforated Base. *J. Mar. Sci. Eng.* **2022**, *10*, 1205. [[CrossRef](#)]
33. Mohapatra, S.C.; Guedes Soares, C. 3D hydroelastic modeling of fluid-structure interactions of porous flexible structures. *J. Fluids Struct.* **2022**, *112*, 103588. [[CrossRef](#)]
34. Mohapatra, S.C.; Guedes Soares, C. Effect of mooring lines on the hydroelastic response of a floating flexible plate using the BIEM approach. *J. Mar. Sci. Eng.* **2021**, *9*, 941. [[CrossRef](#)]

Disclaimer/Publisher’s Note: The statements, opinions and data contained in all publications are solely those of the individual author(s) and contributor(s) and not of MDPI and/or the editor(s). MDPI and/or the editor(s) disclaim responsibility for any injury to people or property resulting from any ideas, methods, instructions or products referred to in the content.